Structure-properties relationships in fibre drawing of bioactive phosphate glasses

Laura Muñoz-Senovilla[1], Francisco Muñoz[1,*], Gregory Tricot[2], Ifty Ahmed[3], Andrew J. Parsons[3]

[1]*Ceramics and Glass Institute (CSIC), Kelsen 5, 28049 Madrid (Spain)*

[2]*LASIR UMR CNRS 8516, Université de Lille 1, 59655 Villeneuve d'Ascq Cedex (France)*

[3]*Faculty of Engineering, University of Nottingham, Nottingham NG7 2RD (United Kingdom)*

*Corresponding author:

E-mail: fmunoz@icv.csic.es

Tel: +34917355840

Fax: +34917355843

Abstract

New bioactive phosphate glasses suitable for continuous fibre production are investigated in this work. The structure of both bulk and fibres from Na_2O-CaO-MgO-P_2O_5 glasses has been studied by means of Raman and ^{31}P and ^{23}Na Nuclear Magnetic Resonance spectroscopies, and the structural results have been correlated with the mechanical properties of the fibres and the dissolution rate of the bulk glasses. It has been observed that the mechanical properties of the phosphate glass fibres are influenced by the glass network connectivity, whilst the dissolution rates are governed by the Q^i speciation of the PO_4 units. As seen in previous studies, molar volume seems to play an important role in the fragility behaviour of phosphate glasses. Here, a lower molar volume resulting from the increase in the oxygen packing density, hinders the cooperative flow of the PO_4 units throughout the glass network and, therefore, causes a reduction in the kinetic fragility.

Keywords: Phosphate Glasses; Fibres; Bioglasses; Structure; Viscosity; Mechanical Properties

1. Introduction

Phosphate-based glass fibres are a class of bioactive glasses that have generated considerable interest due to their potential to be used as active materials, either directly or as reinforcement phase, for resorbable implants and for hard and soft tissue engineering applications [1-4]. Their capacity to dissolve completely in aqueous media, through a surface erosion process that allows the maintenance of properties during degradation [5, 6], and the ability to control their degradation rates and mechanical properties through tailoring the glass composition are valuable properties. However, phosphate glasses present a higher kinetic fragility when compared with silicate glasses, which narrows their fibre drawing temperature range and makes them prone to crystallization when held in this range.

In order to design new bioactive phosphate glasses suitable for continuous fibre production and industrial implementation, it is necessary to determine the glass network structure and a complete knowledge of the viscosity behaviour with temperature. These fundamental studies will allow prediction of the drawing point with enough accuracy to support fibre processing and indicate preferential glass structures. Accordingly, a big effort has been done so far to determine the structure in several bioactive phosphate glasses for fibre drawing by means of Nuclear Magnetic Resonance and Raman spectroscopies [7-9]. But only a few works have been published about structural studies performed directly on the fibres due to the complexity of their determination [7]. More recently, several works have been published on the improvement of processing conditions for fibre drawing based on kinetic fragility determination [10, 11], enhancing the important role of the structure to predict the behaviour of bioactive glasses during processing [12].

In this study, four phosphate glass formulations in the system Na_2O-MgO-CaO-P_2O_5 were selected according to previous formulations that present good cytocompatibility, with magnesium and calcium contents fixed at 24 and 16 mol %. In a previous work, the thermal

properties and the viscosity behaviour of these glasses were studied through combined quasi-static and rotation methods and the theoretical fibre drawing points and fragility of the glasses were determined [11].

In order to highlight the importance of viscosity and structure on the design of bioactive phosphate glasses suitable for fibre drawing, this work aims to relate macroscopic properties, such as kinetic fragility (m) and molar volume (V_m), with the glass fibre structure determined directly by means of Raman and ^{31}P and ^{23}Na Nuclear Magnetic Resonance (NMR) spectroscopy. The structural features will be compared with those observed in the bulk glasses to elucidate if changes in the glass network structure occur during fibre processing. Static ^{31}P nuclear magnetic resonance will be employed also, to obtain experimental evidence of the anisotropy generated on the glass fibre due to the mechanical load applied during fibre drawing. The structural results will be related to empirical observations made during fibre drawing, such as pulling temperature and the ease of continuous fibre manufacture. Additionally, the mechanical properties of the fibres and the dissolution rate of the glasses in phosphate buffered saline (PBS) media will be related to compositional changes in the glass network structure.

2. Materials and methodology

2.1 Glass production

Glasses with compositions $xNa_2O{\cdot}16CaO{\cdot}24MgO{\cdot}(60\text{-}x)P_2O_5$ (x=5,10,15,20) were prepared by conventional melt-quenching technique. Reagent grade raw materials: NaH_2PO_4, $CaHPO_4$, $MgHPO_4.3H_2O$ (Sigma Aldrich UK) and P_2O_5 (Fisher Chemicals) were mixed in appropriate ratios. Batches were placed into a platinum-gold crucible and heated for 30 min at 350ºC in an electric furnace to drive off adducted water, before being melted at 1100ºC for 90 min. The melts were either cast directly onto a steel plate or poured into 9 mm graphite moulds.

The glasses were annealed at 10ºC above their glass transition temperature before sectioning into parallel faced, ~10mm long rods for durability tests.

2.2 Glass characterization

Glass density was measured by helium pycnometry in a Micromeritics AccuPyc 1330 on bulk samples (±1 $Kg.m^{-3}$). The molar volume (V_m) was calculated by using the relation between the molar mass (M) and the density (ρ) of the glass ($V_m=M\cdot\rho^{-1}$).

^{23}Na magic angle spinning (MAS) NMR was performed on a Bruker *Avance II* spectrometer operating at 105.87 MHz (9.4 T). The pulse length was 2 μs (corresponding to a $\pi/6$ flip angle) and a 2 s delay time was used. A total number of 256 scans were accumulated at a spinning rate of 12.5 kHz on the bulk glass. NaCl 1M was used as reference. The ^{23}Na NMR spectra were simulated with the Dmfit software [13] using the Czjzek [14] distribution models.

^{31}P MAS-NMR spectra were recorded on a *Bruker Avance II* spectrometer operating at 161.96 MHz (9.4 T). The pulse length was 2 μs (corresponding to a $\pi/5$ flip angle) and a 120 s delay time was used. A total number of 32 transients were accumulated with a spinning rate of 12.5 kHz for the bulk glass and 10 kHz for the fibres due to stability reasons. The ^{31}P MAS NMR spectra were fitted with Gaussian functions, in accordance with the chemical shift distribution of the amorphous state. Static ^{31}P NMR experiments were recorded with 64 transients and a 15 s delay in order to determine the chemical shift anisotropy (CSA) parameters. Solid $(NH_4)H_2PO_4$ was used as secondary reference with a chemical shift of 0.82 ppm with respect to H_3PO_4 (85 %).

Raman spectroscopy analyses were performed on both bulk samples and single fibres on a *Witec Alpha300RA* Raman-AFM confocal spectrometer with 532 nm laser wavelength excitation and 39 mW power in the range of 220-3800 cm^{-1}. The laser polarization angle was located along the x-axis and microscope lens of 100 augments was used in all cases. The focus was adjusted to lie well beneath the surface of a single fibre in order to avoid any possible degradation on the fibre surface due to ambient moisture. The precision in the determination of the Raman shifts is ± 1 cm^{-1}.

2.3 Degradation studies

Degradation tests via hydrolysis were performed according to the standard BS EN ISO 10993-13:2010 on three replicate samples per glass composition, each sample being ~ 9 mm diameter and 10 mm length. The annealed samples were placed laid on their side at the bottom of the vial into 30 ml glass vials filled with phosphate buffered saline solution (PBS) (pH = 7.4±0.2) as degradation medium, and maintained at a constant temperature of 37°C. The samples were blot dried at each time point before taking weight and dimensional measurements. The time points that were used were 1, 3, 7, 14, 21, 28, 42, 56 and 84 days. After each time point measurement the solution was discarded and replaced with fresh PBS solution in order to maintain the pH. Before discarding the solution, the pH was measured in order to check for deviations in pH during the degradation test. Glass degradation has been expressed in terms of dissolution rate (D_R) by equation (1):

$$D_R = (m_i - m_d)/(SA \cdot t) \qquad (1)$$

where m_d is the mass of degraded sample, m_i is the initial mass of the sample, SA is the sample surface area and t is the degradation time.

2.4. Glass fibre production

Continuous fibres with diameters ranging from approximately 10 to 25 μm were produced via a melt-draw spinning process using a dedicated in-house facility. The speed was varied from 780 to 1620 rpm for each composition, in order to ensure fibres were obtained with similar diameters for strength comparison. The pulling temperature was adjusted to approximately 150ºC above the liquidus temperature in order to overcome the temperature gradient between the thermocouple controller and the actual temperature at the bottom of the platinum crucible.

2.5 Single Fibre Tensile Test (SFTT)

Tensile testing of single filaments was conducted in accordance with BS ISO 11566 by using a single fibre tensile tester *Diastron LEX-810* (UK) at room temperature with a load capacity of 0.2 N and a speed of 0.017 $mm \cdot s^{-1}$. A laser scan micrometre *Mitutoyo LSM6200* attached to the tensile tester was employed prior to testing for the determination of the individual fibre diameter. The laser scan micrometre was calibrated with phosphate glass fibres of known diameters previously determined by SEM. The precision in diameter determination is considered to be ± 0.3 μm. At least 40 fibres were tested with a gauge length of 25 mm. Tensile strength (δ_f) and tensile modulus (E_f) were calculated following equations (2) and (3):

$$\delta_f = F_f/A_f \quad (2)$$

$$E_f = [(AF/A_f)\cdot(L/\Delta L)]/[1-K(\Delta F/\Delta L)] \quad (3)$$

F_f is the maximum tensile at break of the fibre and A_f is the cross-section area of the filament. On the other hand, ΔF and ΔL are the respective differences in force and length corresponding to the strain limits selected in accordance with BS ISO 11566 and depending on the nominal strain at break of the fibre, with L being the gauge length and K the system compliance.

The effect of composition on the tensile strength and tensile modulus was studied. Due to the brittle character of phosphate based glass fibres, a Weibull distribution was employed to statistically characterize the failure mode of the fibres via the statistical software Minitab ® 15.

3. Results and discussion

3.1 Structural Characterization

3.1.1 Magic Angle Spinning Nuclear Magnetic Resonance (MAS-NMR)

The ^{23}Na and ^{31}P MAS NMR spectra of the $xNa_2O.16CaO.24MgO.(60\text{-}x)\ P_2O_5$ glass series are depicted in Figure 1a) and b), respectively.

The distribution of Na^+ ions within the structure of $xNa_2O{\cdot}16CaO{\cdot}24MgO{\cdot}(60\text{-}x)P_2O_5$ glasses can be analysed by means of ^{23}Na MAS NMR. The spectra (Fig. 1a) present a characteristic shape associated to the Second Order Quadrupolar Effect (SOQE) in distributed structures. This system cannot be simulated with a Gaussian model because it is not capable of reproducing this asymmetry coming from the quadrupolar parameters distribution. Simulations have thus been carried out using the Czjzek model [14]. The NMR parameters deduced from the spectra simulation, such as chemical shift and quadrupolar constant (C_Q), are reported in Table 1. The evolution of the chemical shift towards higher frequencies (lower field) is usually related with small and continuous changes on the cation coordination sphere towards lower coordination number (CN), but investigations in binary lithium phosphate glasses [15] have discussed that correlations between the observed chemical shift and the structure usually does not depend only on one factor since the chemical shift ranges for different CN overlap. Thus, a variety of structural parameters such as coordination number, bond length and modifier ion nature should be involved. For example, ^{23}Na NMR investigations of silicate and alumina-silicate crystals and melts have shown that a decrease

in the degree of network polymerization within the structure produces an increase in the ^{23}Na chemical shift [16]. The phosphate glasses show a different trend, where the variation in C_Q is not significant, suggesting that the chemical environment around the sodium cations is constant. These results indicate that the Na^+ ions are distributed around the phosphate units independently of the former oxide content and thus of the glass composition.

The evolution of the phosphate network is monitored by ^{31}P NMR in Fig. 1b. Three signals can be observed at -42 ppm, between -30 and -20 ppm and at -5 ppm. These three resonances are attributed to different Q^i sites. Since less shielded signals indicate an electronic density redistribution around phosphorous (with changing bridging to non-bridging oxygen), the three signals can be assigned to Q^3, Q^2 and Q^1 site in a good agreement with previous studies [17]. In order to study the evolution of Q^i units as a function of composition and to compare them with the theoretical values, the relative fraction of each species has been plotted as function of Na_2O molar percentage in Figure 2. It can be observed that, as expected, Na_2O content increases the glass network depolymerisation. Progressively, the presence of Q^i units with fewer bridging oxygens, i.e. Q^1, occurs at the expense of Q^3 and Q^2 groups. For both the bulk glass and the fibres, the relative speciation is very close to the theoretical values predicted by the structural model based on the nominal composition that was described following the work of Van Wazer [18] and is represented by equations (4) and (5), where x represents the molar fraction of a modifier oxide in a glass with general composition $x(R_2O$ or $R'O)$-$(1-x)P_2O_5$:

$$f(Q^2)=x/(1-x);\ f(Q^3)=(1-2x)/(1-x) \text{ where } 0\leq x\leq 0.5 \quad (4)$$

$$f(Q^1)=(2x-1)/(1-x);\ f(Q^2)=(2-3x)/(1-x) \text{ where } 0.5\leq x\leq 0.67 \quad (5)$$

In general, it can be observed that the glass network structure in the fibres slightly differs from that of the bulk. The proportion of Q^1 groups is slightly higher in the fibres than in the

bulk glasses at the expense of Q^2 groups' proportion. It is worth noting that for metaphosphate glass fibres composition (x=10), where the tetrahedral units should be of Q^2 type (except for a small proportion of Q^1 ending groups), a low but not negligible proportion of Q^3 groups appear. The presence of these species could be caused by a disproportionation reaction of the type of Q^2 groups into Q^1 and Q^3 units, causing the appearance of Q^1 and Q^3 units when compared with the bulk glass. The reaction is described in equation (6) [18]:

$$2Q^2 \leftrightarrow Q^1 + Q^3 \tag{6}$$

Q^1 site disproportionation reactions are usually observed in pyrophosphate glasses, though a case of Q^2 disproportionation has also been reported in a calcium metaphosphate composition [19].

The relative speciation of Q^i units has been used to calculate the experimental P_2O_5 molar fraction present in the glass through equations (4) and (5). The values obtained are equal to the nominal ones, except for the x=10 where a deviation of 2 mol % on the P_2O_5 content has been observed. The experimental molar fraction of P_2O_5 has been used to calculate the network connectivity of the glasses (NC), defined as the number of bridging oxygens (BO) per network forming element [20], the average chain length (ñ) according to Bunker et al. [20], as well as the oxygen packing density [O] in the glass [21]. NC, ñ and [O] were calculated according to equations (7), (8) and (9), respectively:

$$NC = \frac{3[P_2O_5] - [M_2^{I}O] - \sum[M^{II}O]}{[P_2O_5]} \tag{7}$$

$$\bar{n} = \frac{2}{\frac{[M_2^{I}O] + \sum[M^{II}O]}{[P_2O_5]} - 1} \tag{8}$$

$$[O] = \frac{1000.\rho(O)}{M} \quad (9)$$

where $[M_2^{I}O]$ and $[M^{II}O]$ are the molar fractions of the network modifiers and $[P_2O_5]$ is the molar fraction of phosphate network forming oxide. ρ is the density of the glass, (O) is the number of oxygen atoms in the glass composition and M is the molar mass of the glass.

The values obtained and represented in Figures 3 and 4 are close to the nominal ones due to the similarity between the experimental and the nominal composition.

As seen in the ^{31}P MAS-NMR spectra, the replacement of P_2O_5 by Na_2O causes network depolymerisation. Progressively, the increase of the Q^i units with fewer bridging oxygens, i.e. from Q^3 to Q^2 and Q^1, results in shorter phosphate chains and lower network connectivity as Figure 3 shows. The depolymerisation caused by the addition of Na_2O as modifier oxide induces a contraction of the glass network that leads to the densification of the glass and thus to a decrease in the volume occupied by one mole of glass, as depicted in Figure 4. The subsequent increasing amount of Na^+ will force these ions to share the available NBO, resulting in coordination polyhedra that have to share corners and edges increasing the oxygen packing density (cf. Fig. 4).

The ^{31}P chemical shift anisotropy (δ_{CSA}) provides information about the conformation of the Q^i units. δ_{CSA} was determined from the integration of the MAS NMR spectra including the spinning sidebands using dmfit software [13]. Larger values of this tensor are found in structures in which there is a prevalence of rings arrangements instead of phosphate chains [17, 22]. In Table 2 the δ_{CSA} values obtained for the fibres and bulk glasses for Q^2 units are collected.

According to our results, the chemical shift anisotropy is similar for the bulk and glass fibres and does not vary between the meta- and x=15 pyrophosphate glass. In both, the Na rich glass compositions seem to favour chain structures.

Bulk glasses are isotropic materials with respect to their structure and physical properties. However, they can develop a certain degree of anisotropy as a result of the stress applied during conversion into glass fibres.

In the past, the orientation and alignment of the weakest bonds within the glass structure along the axis of the fibre have been discussed. Goldstein and Davies developed the concept of glasses as polymers consisting of glass forming atoms connected by oxygen that allows the formation of fibres with oriented linear chains, based on the similarity found between diffraction patterns of sodium metaphosphate glass fibres and organic fibres with oriented chain molecules [23]. Subsequently, Milberg and Daly investigated the structure of fibres made from the same glass composition and the results indicate that the sodium metaphosphate fibres were made up of long chains that are preferentially orientated along the fibre main axis, thus a strong structural anisotropy results from the rearrangements of the structural units [24]. Furthermore, Muñoz *et al*. [25] have studied the anisotropy of phosphate glass fibres through the measurements of optical birefringence and have correlated it with the drawing stress and the diameter of the drawn fibre. A permanent birefringence is observed in the case of glass fibres drawn by applying high shear stresses as a consequence of the alignment of anisotropic flow units.

With the aim of studying if any favoured direction is taken by the chains present in the glass structure, and thus corroborating the studies discussed above for these particular compositions, the anisotropy of the metaphosphate glass (i.e. x=10) has been studied using Static Nuclear Magnetic Resonance of ^{31}P. The spectra of both the bulk glass and the fibres are depicted in Figure 5. It can be observed that there is almost no difference between the spectra, thus the variation in the chemical shift anisotropy (δ_{CSA}) that should be observed as a consequence of phosphate chain alignment does not seem to be reflected in the phosphorous local environment. Additionally, the δ_{CSA} obtained from the simulation of the rotation bands

in the ^{31}P MAS NMR spectra of the bulk glass and fibres, -131 ppm and -130 ppm respectively, does not shed light on the discussion. On the other hand, the line shape of the minor amount of Q^1 units present in the glass, as discussed above, will overlap with the Q^2 dominating pattern. Braun et al. [26] have studied extruded calcium metaphosphate glasses by static and 2D MAS NMR. As in these glasses, they conclude that it is almost impossible to verify a noticeable local structural alignment of the phosphate chains in the glass fibres with ordinary static NMR.

Furthermore, it is known that different cooling rates might have a strong influence on the fictive temperature of the fibers [27]. Within the scope of the present study we have not looked at specific cooling rates in a wide enough range as that would be quite difficult to determine in a drawn fiber. It is likely that the bulk glass and fibers have different fictive temperatures though being highly difficulty to estimate a cooling rate for the fiber drawing process we have not attempted here to quantify its effect. In any case, we cannot elucidate whether the chains of PO_4 tetrahedra present in the glass fibres are randomly distributed or lie along the fibre main axis direction, but the good mechanical properties observed in these fibres that will be discussed in detail in section 3.3 may suggest that a structural orientation of the fibres is taking place.

3.1.2 Raman Spectroscopy

Raman spectroscopy was employed as a complementary method to study the structure of the bulk glasses and that of the fibres, specifically to determine if any changes occurred in the active vibrational modes of phosphorous to oxygen bonds. Figure 6 shows the Raman spectra collected for the bioactive glasses. All the spectra were normalized to the band with the greatest intensity. The evolution of the structure with increasing modifier oxide agrees with the observations from ^{31}P MAS-NMR. The spectra are all dominated by two main bands

appearing at about 700 cm^{-1} and 1170 cm^{-1}, attributed to the symmetric stretching modes of phosphorous to bridging (P-O-P) and to non-bridging oxygen bonds (O-P-O) in Q^2 units, respectively [28, 29]. The corresponding asymmetric modes appear as shoulders at ca. 790 cm^{-1} and 1260 cm^{-1} [28, 29]. The progression from a higher cross-linked Q^3 network to a glass network based on chains or rings made up of Q^2 units and a depolymerised glass with the presence of Q^2 units and Q^1 (not only as a chain terminal groups but forming pyrophosphate units) as the [O]/[P] ratio increases, can be followed by observing two significant bands. The band attributed to O-P-O bonds in Q^1 units (~1050 cm^{-1}) gradually increases in intensity and gets broader, while the band attributed to the symmetric stretching mode of P=O bonds in Q^3 groups (~1300 cm^{-1}) progressively disappears. Additionally, the P-O bond bending mode of Q^2 and Q^1 units appears as a broad signal in the range of 200 cm^{-1} to 400 cm^{-1} [28, 29]. If we look at the frequency of the dominant stretching modes of phosphorous linked to non-bridging oxygens from x=5 to x=20, we can observe a progressive change from the mode attributed to P=O bonds in Q^3 to the ones of O-P-O links in Q^2 and further in $P\text{-}O^-$ in Q^1 groups. This is an indication of the depolymerisation of the phosphate network, as has also been seen by NMR, and which is related to the progressive weakening of the bonds between phosphorous and non-bridging oxygens upon sodium addition.

Comparing the structure of the bulk glass and the fibres, no significant difference is observed between the main peaks, either in Raman shift or in intensity. Apart from the higher background present in all the fibres spectra compared with the bulk, the bands attributed to asymmetric modes and the $O\text{-}P\text{-}O_{sym}$ mode in Q^2 units seem to present a higher relative intensity in the fibres than in the bulk, but it is complex to extract conclusions from that observation due to the difference in the background within the Raman shift range mentioned before.

3.2 Glass solubility

While the poor chemical durability of phosphate glasses in aqueous environments has restricted their industrial applications, it was one of the main motivations for their use as temporary bone fracture fixation devices. The dissolution rate of phosphate glasses depends on the chemical composition, the thermal history and the ratio of surface area to volume, but also on the pH of the degradation medium and the degradation temperature [30].

After 84 days of experiment, a decrease in dissolution rate was observed with increasing Na_2O content, as depicted in Figure 7. This trend is reflected in the pH values at each time point, with slightly lower values observed for the faster degrading glasses (average pH at solution change for x=5 was 7.22, for x=10 it was 7.30, for x =15 it was 7.33 and for x=20 it was 7.34, c.f. PBS initial pH of 7.4). The dissolution rate values are in the range of glasses studied previously that have a similar composition [31]. It has been suggested by Parsons *et al.* that a degradation rate of around $5x10^{-10}$ $Kg{\cdot}m^{-2}{\cdot}s^{-1}$ or lower is required for phosphate glass fibres for bone repair applications [32]. The most durable glass found in this study, x=20, is in the range of the suggested optimum rate of performance.

The chemical durability of phosphate glasses is strongly affected by the field strength of the modifying cations and by the glass former oxide proportion. The glasses under study differ in P_2O_5 content, replacing the glass former oxide by Na_2O while CaO and MgO proportions are kept constant. Brauer *et al.* found that the degradation rate of phosphate based glasses is reduced by two orders of magnitude as the P_2O_5 content was reduced from 50 to 45 mol % [33]. Furthermore, the solubility in both the polyphosphate and the pyrophosphate regions was also investigated by Vogel *et al.* [34-36], whom results suggested that phosphate invert glasses were more resistant to hydrolysis than the chain structure of meta- and polyphosphate glasses. In general, these authors observed that a reduction in degradation rate occurs with decreasing P_2O_5 content and suggest that the depolymerisation of the phosphate chain

structure and formation of Q^1 groups make the glasses less susceptible to hydration as in the present case. As seen in the structural characterization, with increasing Na_2O content the glass network depolymerises. The proportion of Q^1 units increases at the expense of Q^3 and Q^2 groups, thus increasing the resistance to dissolution. Phosphate glass with 55 P_2O_5 mol % (x=5) has the highest dissolution rate with a value of 1.7 10^{-9} $Kg \cdot m^{-2} \cdot s^{-1}$. This can be explained based on the presence of potentially hydrolysable P-O-P bonds in Q^3 groups for this glass composition. In the meta- and polyphosphate region the dissolution rate decreases with decreasing former oxide. As discussed above, the decrease in the fraction of more hydrolysable Q^2 species, along with an increase on the oxygen packing density decreases the dissolution rate and thus enhances the chemical durability.

3.3 Mechanical properties of glass fibres

Phosphate glass fibres are brittle in nature, as it is seen by their low values of strain to failure. Figure 8 summarises the effect of increasing Na_2O on the mechanical properties of glass fibres such as tensile fracture stress and modulus. A decrease in tensile fracture stress was seen with increasing Na_2O content. The best mechanical properties of the phosphate glass fibres tested are given by the glass with higher network connectivity and lower oxygen packing density that corresponds to the glass with higher phosphate content (x=5). This is consistent with previous results obtained in similar bioactive glass systems [31]. The tensile modulus of a material is an intrinsic property and should follow the same trend as tensile fracture, but in the glasses under study the moduli of x=20 shows the highest value. The shorter chains present in this glass composition, as ñ shows, will be able to pack together tighter and thus create a more durable glass with greater tensile modulus.

As it can be seen in Figure 8, the average diameter of the fibres is quite similar for x=5 to x=15, however the glass fibres with 40 mol % of P_2O_5 (x=20) were thicker. Although

multiple speeds were used in order to obtain fibres with comparable diameters, it was not possible to draw this fibre type successfully at a small enough diameter. The average diameter is about 10 μm higher for x=20 and this could contribute to the reduced strength values. However, the fibre diameter is not the only factor that could have an impact on the tensile strength. Lund *et al.* [37] argued that the glass structure could influence the normal strength of glass fibres in a different way. As is it known, the structural anisotropy of continuous glass fibres, i.e. orientation of structural units along the fibre axis, increases with the drawing speed, and enhances their tensile strength. As explained above, the fibres selected were those with closer diameters to the ones found for the remaining glass compositions. This could indirectly involve the selection of fibres drawn at the higher speeds due to the inverse relation between drawing speed and continuous fibre diameter, and therefore imply a higher structural anisotropy on these fibres that finally results in the comparably low strength of the x=20 glass.

The Weibull distribution is a well-known and accepted statistical tool used to characterize the failure mode of brittle fibres [38]. Weibull modulus (m) indicates the fibre reliability. If this parameter takes large values, then the failure is predictable. However, a low Weibull modulus would introduce uncertainty about the strength of the fibre [39]. Weibull modulus and normalising stress for the bioactive glass fibres, together with the tensile fracture stress values are collected in Table 3.

As it can be observed, the trend of normalising strength (σ_0) is consistent with the trend of average tensile fracture strength. The glass fibres of x=15 glass present the highest Weibull modulus among the glass systems under study, closely followed by the x=5 glass fibres, and is therefore the most reliable fibre. Furthermore, the highest value of tensile fracture stress is obtained for x=5 glass fibres, i.e. 55 mol % P_2O_5. Therefore, the glass composition that

shows the best compromise between both Weibull modulus and tensile fracture stress is that of the glass fibres with highest former oxide content, x=5 glass.

3.4 Kinetic fragility and fibre drawing ability

The fragility values that are going to be discussed here in terms of the structural features have been calculated from experimental viscosity data as determined by rotation and quasi-static viscosity methods along the high and low temperature range, respectively [11]. The values are reproduced in Figure 9 for convenience. The combination of these two techniques allows for the experimental determination of viscosities within the processing range up to 10^8 Pa·s and on the melt. Based on the conclusions obtained from previous viscosity studies in phosphate glasses [40, 41] and on Angell's kinetic fragility definition [42], the absence of viscosity data on the transition range may underestimate the fragility values obtained from the fits, in this case to Vogel-Fulcher-Tamman equation (VFT). However, the trend followed with composition is expected to be similar even if the values may vary. As discussed in the work where these data are published [11], fragility results are somewhat unexpected. Lower network connectivity and thus a larger concentration of NBO together with a decrease in the phosphate chain length with increasing modifier content, would give rise to an increase of the kinetic fragility since it would take less time for the shorter chains to rearrange and relax. However, fragility decreases from metaphosphate composition (x=10) to x=20. The variation observed with composition could be caused by the glass network compaction degree. A higher proportion of short chains arrangements, as δ_{CSA} and ñ values showed, would lead to a denser glass network, as the increase on the oxygen packing density with increasing alkali content shows. The subsequent lower V_m may hinder the cooperative flow of the PO_4 units through the glass network and therefore cause a reduction of the kinetic fragility. Furthermore, the presence of Q^3 units in the x=5 glass, as seen from the structural

determination by spectroscopic techniques, gives rise to a more branched and interconnected glass network that should be responsible for the significantly lower value of fragility. However, as suggested above, this value could be underestimated when taking into account experimental viscosity values nearby the transition range, and thus the drop on fragility could be less pronounced.

The fibre drawing ability of phosphate glasses strongly depends on the structure of the glass, in particular its Q^i speciation [43]. As ^{31}P MAS NMR spectra have shown, no significant changes occur in the glass network structure during fibre drawing. Therefore, the properties or structural features determined in the bulk glasses are applicable to the fibres structure. A less fragile behaviour will lead to a wider temperature window range for fibre drawing since the glass will have a lower tendency to crystallize. This extended temperature range together with compositions with elevated average chain length, i.e. glasses with a structure heavily dominated by Q^2 species, should provide a glass that is easier to draw into fibres. In this work, the fibre drawing was carried out by varying the temperature to modulate the glass flow coming through the crucible filament. With increasing alkali content, the optimum temperature required to draw continuous glass fibres gets lower. Glass compositions x=10 and x=15 were the easiest to draw into fibres because of their polymeric nature due to the high proportion of Q^2 groups. Fibre drawing was almost continuous and gave around 80% and 60% conversion of glass into fibre, respectively. However, it was also possible to draw fibres from x=5 and x=20 glass compositions, which present the lowest kinetic fragility values of the glass series under study (c.f. Fig. 9).

It is worth noting that even though it was challenging, fibres were continuously drawn from the x=20 glass composition (40 mol % P_2O_5). In order to avoid crystallization around crucible filament, it was necessary to increase the temperature around 50 degrees above the optimum value required to keep the glass flow under control. The greater flow achieved could be the

main reason for the higher diameters observed for the x=20 fibres, as discussed in section 3.3. Even though the glass with x=5 presents a lower proportion of Q^2 groups compared with metaphosphate composition, it has Q^3 groups that provide a higher degree of connectivity and a higher tensile strength. These glass network structural features may contribute to withstand the stress from the pulling process, even at the high temperatures employed to draw the fibres due to the higher viscosity of a glass with 55 mol % of P_2O_5.

4. Conclusions

The structural studies performed in the bulk glasses and on the fibres by means of ^{31}P and ^{23}Na MAS NMR and Raman spectroscopies have shown that no significant differences occur in the glass network structure during fibre drawing, especially with respect to the Q^i speciation and to the nature and orientation of the P-O bonds.

A decrease in dissolution rate was observed with increasing Na_2O content, with the glass containing 40 mol % P_2O_5 being the most durable due to the presence of less hydrolysable Q^1 units in the glass network and an increase in the oxygen packing density. Conversely, the glass with the highest P_2O_5 content shows the best mechanical properties with good reliability, according to Weibull distribution studies.

With increasing Na_2O content, a denser glass network as a result of a higher proportion of short chains arrangements, will hinder the cooperative flow of the PO_4 units through the glass network and therefore cause a reduction in the kinetic fragility. This lower fragile behaviour leads to a wider temperature window range, thus facilitating fibre drawing processing. However, it has been observed that the glass compositions with higher kinetic fragility were actually the ones that were easier to fibre. In this regard, due to the similar fragility values obtained for the glasses under study, further compositions in the same glass system should be

tested in order to confirm the fragility variation with composition in a wider compositional range.

Acknowledgements

F. Muñoz and L. Muñoz-Senovilla are thankful to the projects MAT2010-20459 and MAT2013-48246-C2-1-P from MINECO of Spain and L. Muñoz-Senovilla also thanks the MINECO for her PhD scholarship (BES-2011-044130). I. Ahmed and A. J. Parsons would like to thank the University of Nottingham for facilitating the hosting of L. Muñoz-Senovilla during her exchange visit. G. Tricot thanks would like to thank Region Nord Pas de Calais, Europe (FEDER), CNRS, University of Lille and TGIR-RMN-THC FR3050 CNRS for funding.

References

[1] Hench L.L, Hench J.W., Greenspan D.C. (2004) Bioglass: a short history and bibliography, J. Aust. Ceram. Soc. 40 (1):1-42.

[2] Knowles J.C. (2003) Phosphate based glasses for biomedical applications, J. Mater. Chem. 13:2395-2401.

[3] Parsons A.J., Ahmed I., Haque P., Fitzpatrick B., Niazi M.I.K., Walker G.S., Rudd C.D., Phosphate glass fibre composites for bone repair (2009) J. Bionic Eng. 6:318-323.

[4] Brauer D.S., Rüssel C., Vogt S., Weisser J., Schnabelrauch M. (2008) Degradable phosphate glass fibre reinforced polymer matrices : mechanical properties and cell response, J. Mater. Sci. Mater. Med. 19:121-127.

[5] Bunker B.C. (1984) Phosphate glass dissolution in aqueous solutions J. Non-Cryst. Solids 64 (3):291-316.

[6] Haque P., Ahmed I., Parsons A.J., Felfel R., Walker G.S., Rudd C.D. (2013) Degradation properties and microstructural analysis of $40P_2O_5$-24MgO-16CaO-$16Na_2O$-$4Fe_2O_3$ phosphate glass fibres, J. Non-Cryst. Solids 375:99-109.

[7] Massera J., Ahmed I., Petit L., Aallos V., Hupa L. (2014) Phosphate-based glass fiber vs. bulk glass: change in fiber optical response to probe in vitro glass reactivity, Materials Science and Engineering C 37:251-257.

[8] Massera J., Vassallo-Breillot M., Törngren B., Glorieux B., Hupa L. (2014) Effect of CeO_2 doping on thermal, optical structural and in vitro properties of a phosphate based bioactive glass, J. Non-Cryst. Solids 402:28-35.

[9] Brauer D. S., Karpukhina N., Law R. V., Hill R. G. (2010) Effect of TiO_2 addition on structure, solubility and crystallisation of phosphate invert glasses for biomedical applications, J. of Non-Cryst. Solids 356:2626-2633.

[10] Döhler F., Groh D., Chiba S., Bierlich J., Kobelke J., Brauer D. S. (2015) Bioactive glasses with improved processing. Part 2. Viscosity and fibre drawing, J. Non-Cryst. Solids 432:130-136.

[11] Parsons A.J., Sharmin N., Shaharuddin S.I.S., Marshall M. (2015) Viscosity profiles of phosphate glasses through combined quasi-static and bob-in-cup methods, J. Non-Cryst. Solids 408:76-86.

[12] Brauer D. S. (2015) Bioactive glasses-structure and properties, Angew. Chem. Int. Ed. 54:4160-4181.

[13] Massiot D., Fayon F., Capron M., King I., Le Calvé S., Alonso B., Durand J. O., Bujoli B., Gan Z., Hoatson G. (2002) Modeling one- and two-dimensional solid-state NMR spectra, Magn. Reson. Chem. 40:70-76.

[14] Czjzek G., Fink J., Gotz F., Schmidt H., Coey J.M.D., Rebouillat J.P., Lienard A. (1981) Atomic coordination and the distribution of electric field gradients in amorphous solids, Phys. Rev. B 23:2513-2530.

[15] Alam T.M., Conzone S., Brow R.K., Boyle T.J. (1999) ^{6}Li, ^{7}Li nuclear magnetic resonance investigation of lithium coordination in binary phosphate glasses, J. Non-Cryst. Solids 258:140-154.

[16] Xue X., Stebbins J.F. (1993) ^{23}Na NMR chemical shifts and local Na coordination environments in silicate crystals, melts and glasses, Phys. Chem. Miner. 20:297-307.

[17] Grimmer A.R., Haubenreisser U. (1983) High-field static and MAS ^{31}P NMR: Chemical shift tensors of polycrystalline potassium phosphates P_2O_5-xK_2O ($0 \leq x \leq 3$), Chem. Phys. Lett. 99 (1983) 487-490.

[18] Van Wazer J.R. (1958) *Phosphorus and its compounds vol. I*, Interscience, New York.

[19] Fletcher J.P., Kirkpatrick R.J., Howell D., Risbud S.H. (1993) ^{31}P Magic angle nuclear magnetic resonance spectroscopy of calcium phosphate glasses, J. Chem. Soc. Faraday Trans. 89 (17):3297-3299.

[20] Hill R. (1996) An alternative view of degradation of bioglass, J. Mat. Sci. Lett. 15:1122-1125.

[21] Baikova L. G., Fedorov Y.K., Tolstoi M. N. (1991) Structural strength of phosphate glasses, Sov. J. Glass Phys. Chem. 16:211-217.

[22] Duncan T.M., Douglass D.C. (1984) On the ^{31}P chemical shift anisotropy in condensed phosphates, Chem. Phys. 87:339349.

[23] Goldstein M., Davies T.H. (1955) Glass fibers with oriented chain molecules, J. Am. Ceram. Soc. 38:223-226.

[24] Milberg M.E., Daly M.C. (1963) Structure of oriented sodium metaphosphate glass fibers, J. Chem. Phys. 39:2966-2973.

[25] Muñoz F., Pritula O., Sedláček J., Rüssel C. (2008) A study on the anisotropy of phosphate glass fibres, European Journal of Glass Science and Technology Part A: Glass Technology, 49(1):47-52.

[26] Braun M., Yue Y.Z., Rüssel C., Jäger C. (1998) Two-dimensional nuclear magnetic resonance evidence for structural order in extruded phosphate glasses, J. Non-Cryst. Solids 241 (2-3):204-207.

[27] Yue Y.Z., Von der Ohe R., Jensen S. L. (2004) Fictive temperature, cooling rate, and viscosity of glasses, J. Chem. Phys. 120 (17): 8053-8059.

[28] Nelson B.N., Exarhos G.J. (1979) Vibrational spectroscopy of cation-site interactions in phosphate glasses, J. Chem. Phys. 71:2739-2747.

[29] Brow R.K., Tallant D.R., Myers S.T., Phifer C.C. (1995) The short-range structure of zinc pyrophosphate glass, J. Non-Cryst. Solids 191:45-55.

[30] Gao H., Tan T., Wang D. (2004) Dissolution mechanism and release kinetics of phosphate controlled release glasses in aqueous medium, Journal of Controlled Release, 96:29-36.

[31] Sharmin N., Parsons A.J., Rudd C.D., Ahmed I. (2014) Effect of boron oxide addition on fibre drawing, mechanical properties and dissolution behaviour of phosphate based glass fibres with fixed 40, 45 and 50 mol % P_2O_5, J. Biomat. Appl. 29 (5):639-653.

[32] Parsons A.J., Burling L.D., Scotchford C.A., Walker G.S., Rudd C.D. (2006) Properties of sodium-based ternary phosphate glasses produced from readily available phosphate salts, J. Non-Cryst. Solids 352:5309-5317.

[33] Brauer D.R., Kraft S.C., Kraft J. (2007) Solubility of glasses in the system P_2O_5-CaO-MgO-Na_2O-TiO_2: Experimental and modelling using artificial neural networks, J. Non-Cryst. Solids, 353:263-270.

[34] Vogel J., Wange P., Hartmann P. (1997) Effect of composition changes on the structure and properties of phosphate glasses in the pyrophosphate region, Glass Sci. Technol. 70:23-27.

[35] Vogel J., Wange P., Hartmann P. (1997) Phosphate glasses and glass-ceramics for medical applications, Glass Sci. Technol. 70:220-223.

[36] Vogel J., Wange P., Knoche S., Rüssel C. (2004) Chemical solubility of phosphate glasses in the system Na_2O-CaO-MgO-P_2O_5-Al_2O_3-TiO_2 in aqueous solutions of different pH values, Glass Sci. Technol. 77:82-87.

[37] Lund M. D., Yue Y.Z. (2010) Impact of drawing stress on the tensile strength of oxide glass fibers J. Am. Ceram. Soc. 93 (10):3236-3243.

[38] Kobayashi H.Y.L.S., Brauer D.S., Rüssel C. (2010) Mechanical properties of a degradable phosphate glass fibre reinforced polymer composite for internal fracture fixation, Mat. Sci. and Eng. C, 30 (7):1003-1007.

[39] Hull D., Clyne T. W. (1996) An introduction to composite materials. NY: Cambridge University Press.

[40] Muñoz-Senovilla L., Muñoz F. (2014) Behaviour of viscosity in metaphosphate glasses, J. Non-Cryst. Solids 385:9-16.

[41] Muñoz-Senovilla L., Venkatachalam S., Muñoz F., Van Wüllen L. (2015) Relationships between fragility and structure through viscosity and high temperature NMR measurements in Li_2O-ZnO-P_2O_5 phosphate glasses, J. Non-Cryst. Solids 428:54-61.

[42] Angell C.A. (1995) Formation of glasses from liquids and biopolymers, Science 267: 1924-1935.

[43] Ahmed I., Lewis M., Olsen I., Knowles J.C. (2004) Phosphate glasses for tissue engineering: Part 1. Processing and characterization of a ternary-based P_2O_5-CaO-Na_2O glass system, Biomaterials, 25 (3):491-499.

Figure captions:

Figure 1: a) ^{23}Na MAS NMR spectra of $xNa_2O{\cdot}16CaO{\cdot}24MgO{\cdot}(60\text{-}x)P_2O_5$ glasses where x denotes the molar fraction of Na_2O oxide, accompanied by simulations (red dotted lines).b) Isotropic signals of ^{31}P MAS NMR spectra of bulk (continuous lines) and fibre (dotted lines) glass.

Figure 2: Relative speciation of Q^i units as function of Na_2O content. Dotted lines correspond to theoretical values obtained from equations (7.6 and 7.7). Note: Q^1 point in glass fibre x=10 and x=20 is not observed due to the overlap with other points.

Figure 3: Network connectivity (NC) and average chain length (ñ) as function of Na_2O content. Dotted lines are drawn as guide for the eyes. Note: equation 7.10 can be only applied for glasses containing 50 mol % or less of P_2O_5.

Figure 4: Molar volume (V_m) and oxygen packing density ([O]) as function of Na_2O content. Dotted lines are drawn as guide for the eyes.

Figure 5: ^{31}P static NMR spectra of $10Na_2O{\cdot}16CaO{\cdot}24MgO{\cdot}50P_2O_5$ in bulk (black line) and fibres (red line).

Figure 6: Raman spectra of $xNa_2O{\cdot}16CaO{\cdot}24MgO{\cdot}(60\text{-}x)P_2O_5$ glasses in bulk (continuous lines) and fibres (dotted lines).Discontinuous coloured lines show the bands attributed to bending (δ) and stretching (ν) vibrational modes of P-O bonds.

Figure 7: Degradation rate of $xNa_2O{\cdot}16CaO{\cdot}24MgO{\cdot}(60\text{-}x)P_2O_5$ glasses in PBS at 37ºC after 84 days. Dotted lines are drawn as a guide for the eyes. Error bars represent the standard deviation of mean value.

Figure 8: Tensile fracture stress, tensile modulus and fibres diameter of the fibres in the glass system $xNa_2O{\cdot}16CaO{\cdot}24MgO{\cdot}(60\text{-}x)P_2O_5$ glasses in PBS at 37ºC after 84 days. Error bars represent the standard deviation. Dotted lines are drawn as a guide for the eyes.

Figure 9: Kinetic fragility as function of Na_2O content. Dotted lines are drawn as guide for the eyes.

Table captions:

Table 1: Chemical shifts and quadrupolar constant (C_Q) extracted from the 1D ^{23}Na NMR spectra simulation. The errors on the values are estimated to ±0.2 ppm and ±0.1 MHz.

Table 2: Chemical shift anisotropy of Q^2 units for bulk and glass fibers. The errors on the values are estimated to ±0.2 ppm.

Table 3: Weibull distribution of fibres in the glass system $xNa_2O{\cdot}16CaO{\cdot}24MgO{\cdot}(60\text{-}x)P_2O_5$.

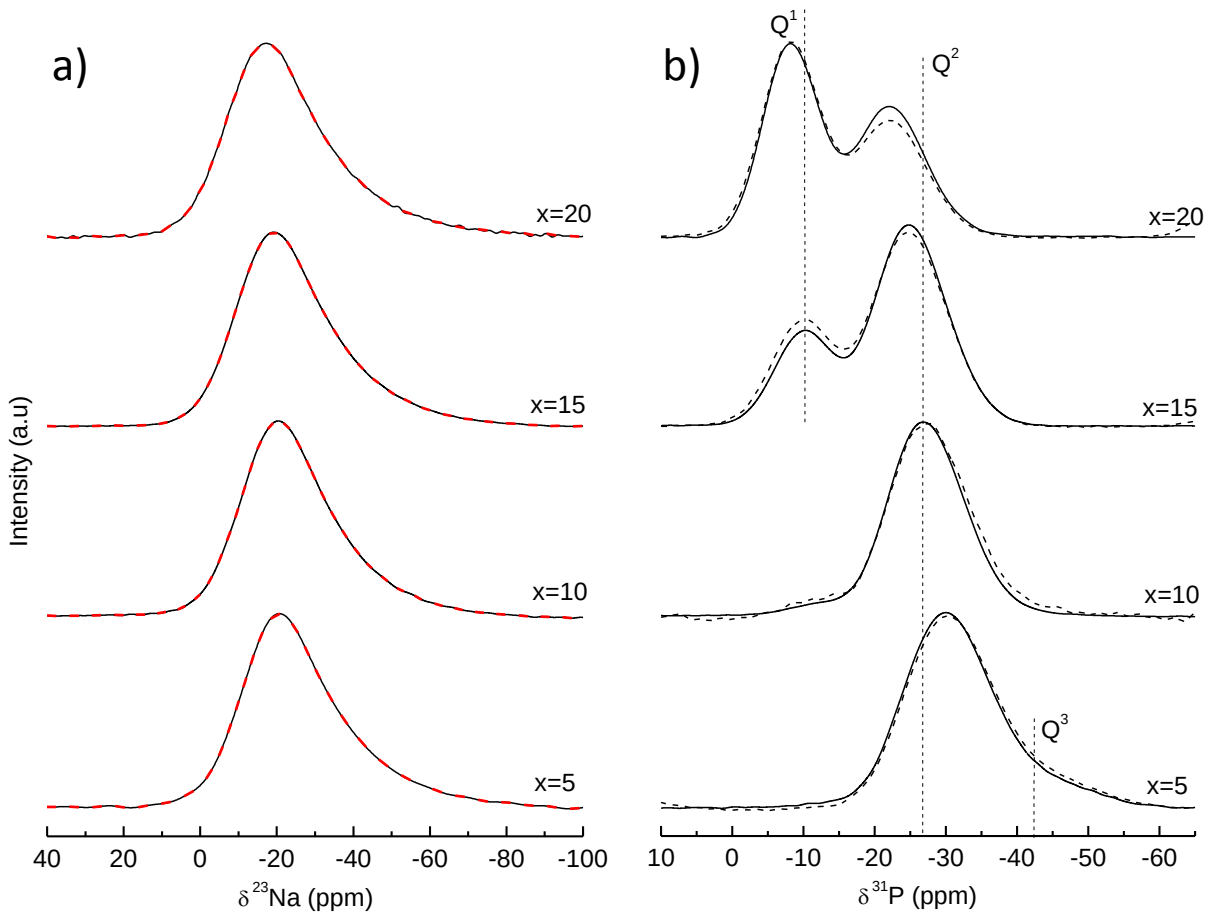
a)
b)
Intensity (a.u)
x=20
x=15
x=10
x=5
Q1
Q2
Q3
40 20 0 -20 -40 -60 -80 -100
δ 23Na (ppm)
10 0 -10 -20 -30 -40 -50 -60
δ 31P (ppm)

Figure 1

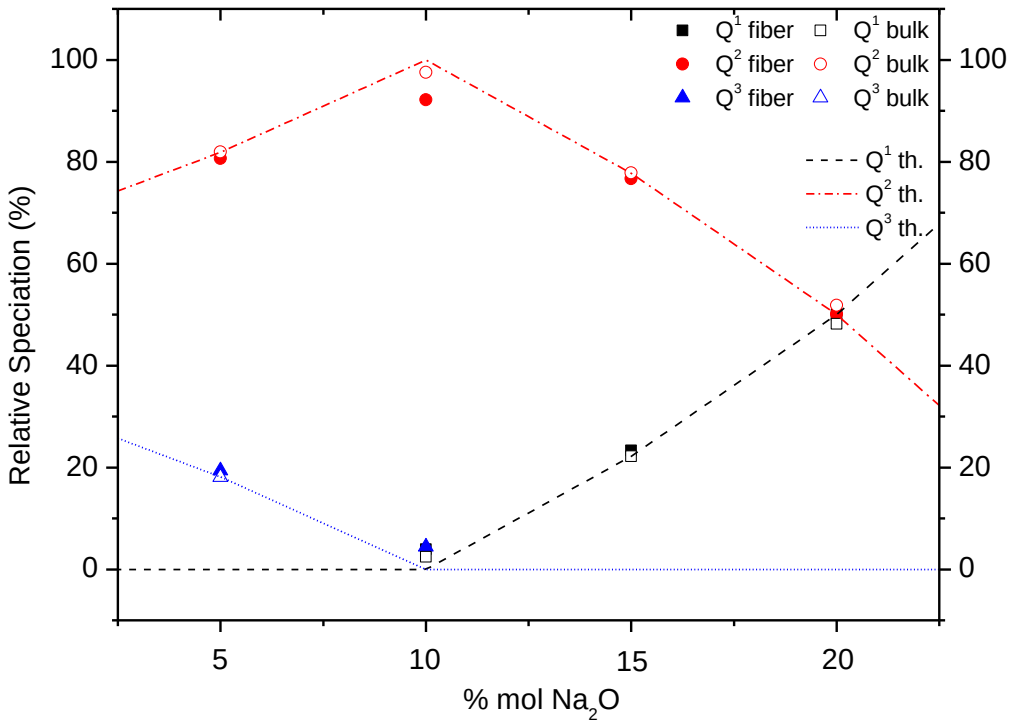
Relative Speciation (%)
% mol Na2O
Q1 fiber
Q2 fiber
Q3 fiber
Q1 bulk
Q2 bulk
Q3 bulk
Q1 th.
Q2 th.
Q3 th.
0
20
40
60
80
100
5
10
15
20

Figure 2

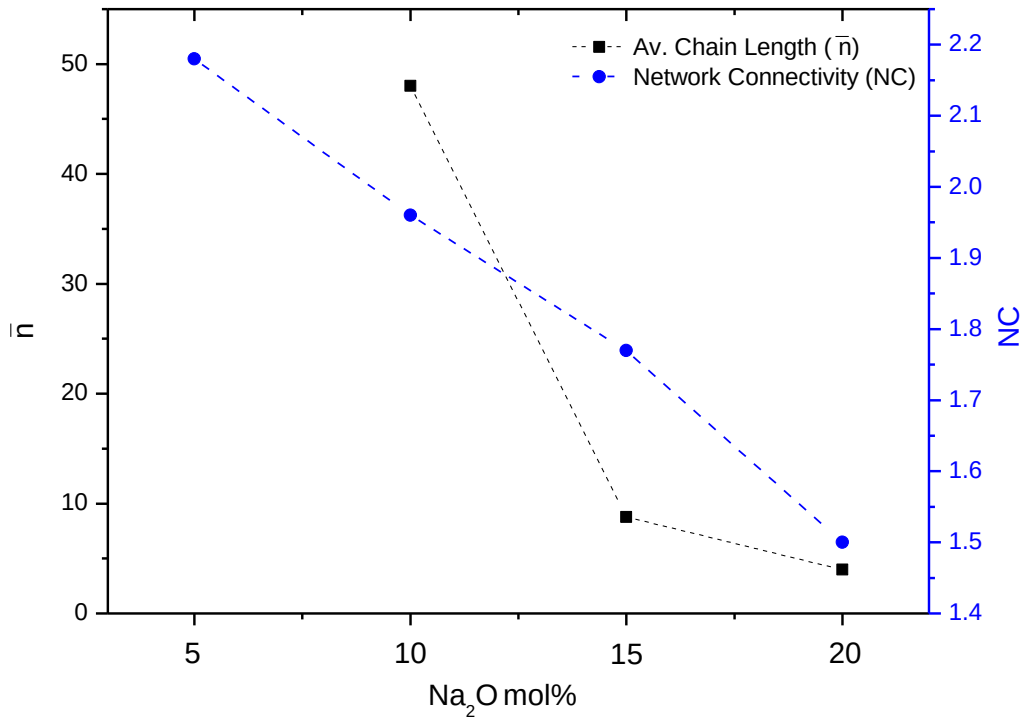
Av. Chain Length (n̄)
Network Connectivity (NC)
n̄
NC
0
10
20
30
40
50
1.4
1.5
1.6
1.7
1.8
1.9
2.0
2.1
2.2
5
10
15
20
Na2O mol%

Figure 3

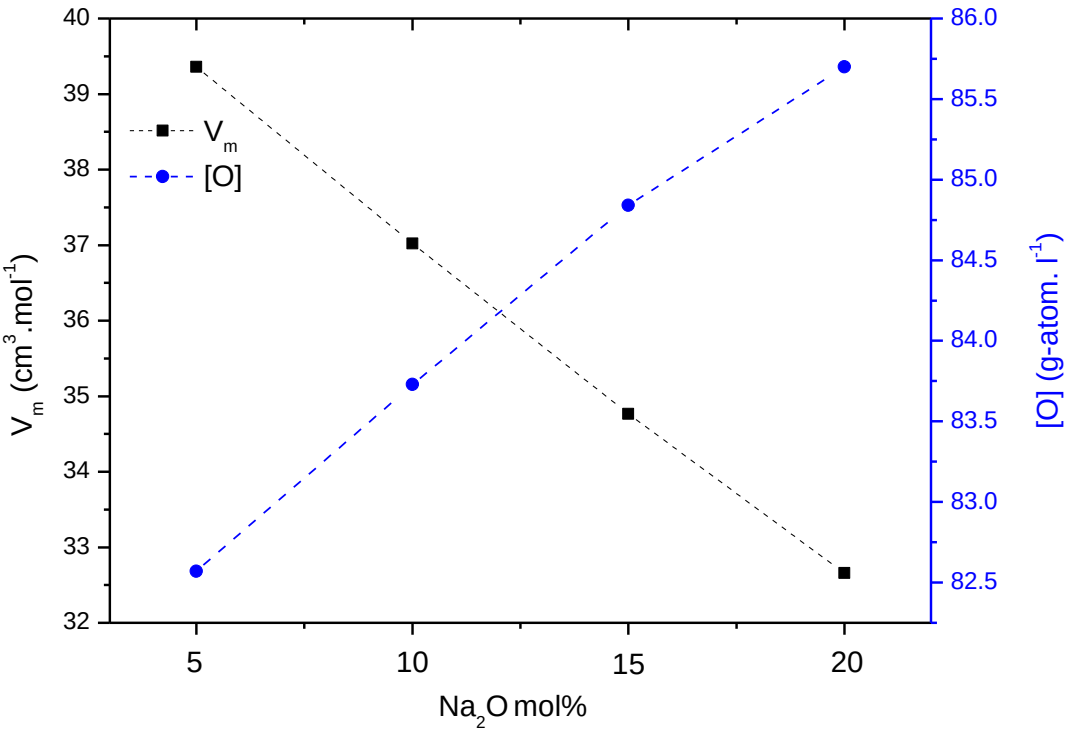
40
39
38
37
36
35
34
33
32
86.0
85.5
85.0
84.5
84.0
83.5
83.0
82.5
5
10
15
20
V_m
[O]
V_m (cm^3.mol^-1)
[O] (g-atom. l^-1)
Na2O mol%

Figure 4

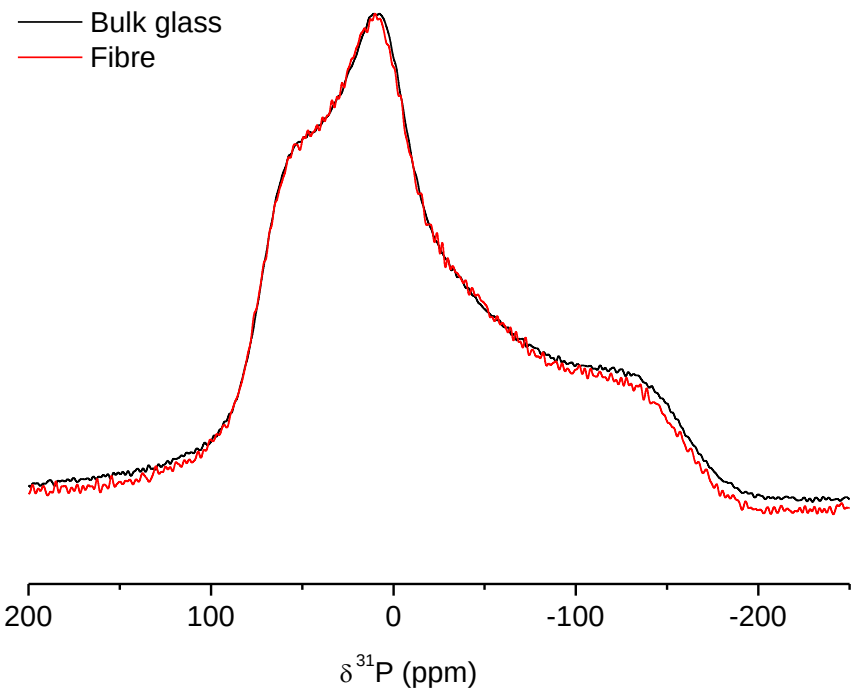

Figure 5

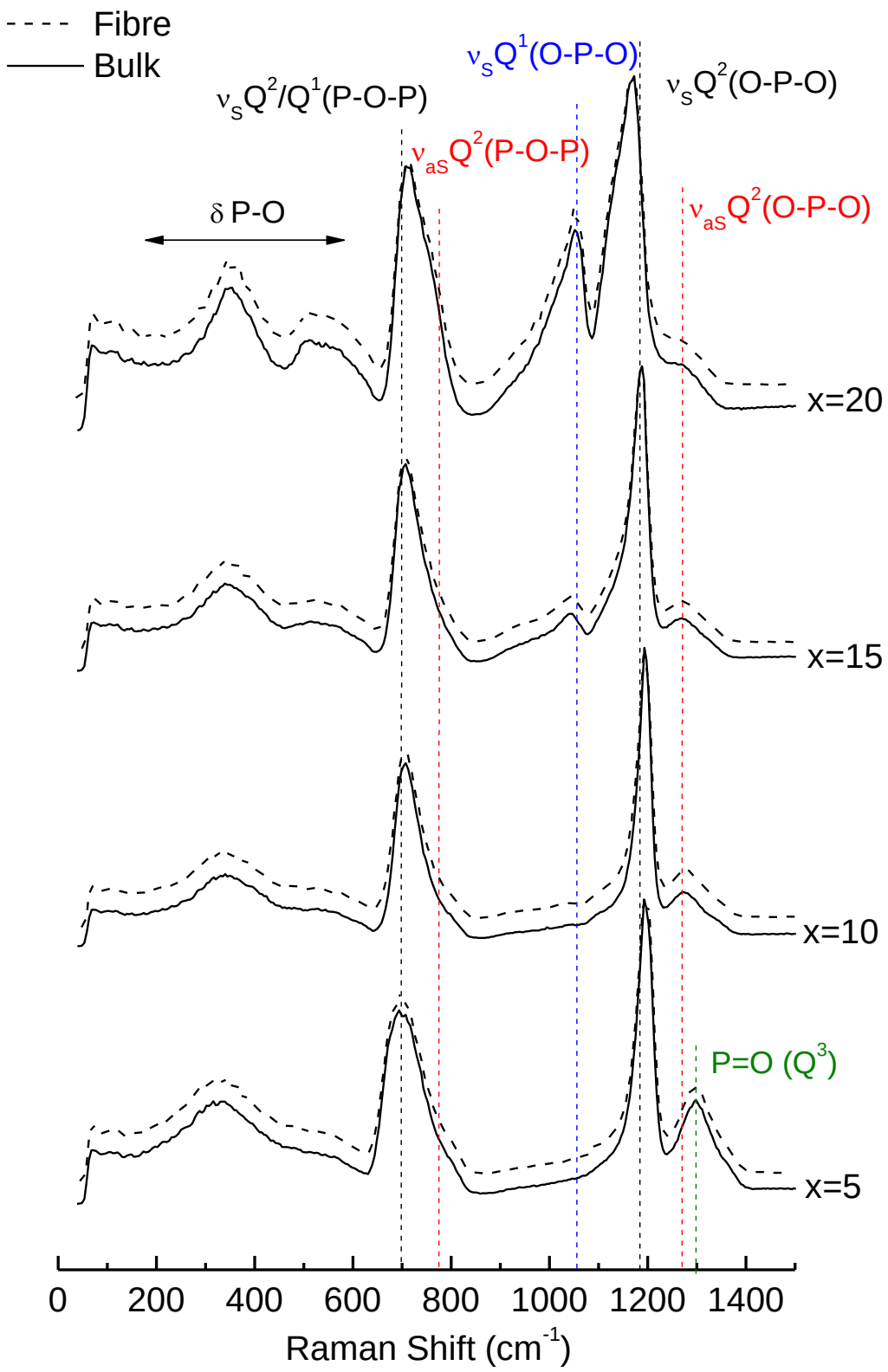
Fibre
Bulk
$\nu_S Q^2/Q^1$(P-O-P)
$\nu_S Q^1$(O-P-O)
$\nu_S Q^2$(O-P-O)
$\nu_{aS} Q^2$(P-O-P)
$\nu_{aS} Q^2$(O-P-O)
δ P-O
x=20
x=15
x=10
P=O (Q^3)
x=5
0
200
400
600
800
1000
1200
1400
Raman Shift (cm^{-1})

Figure 6

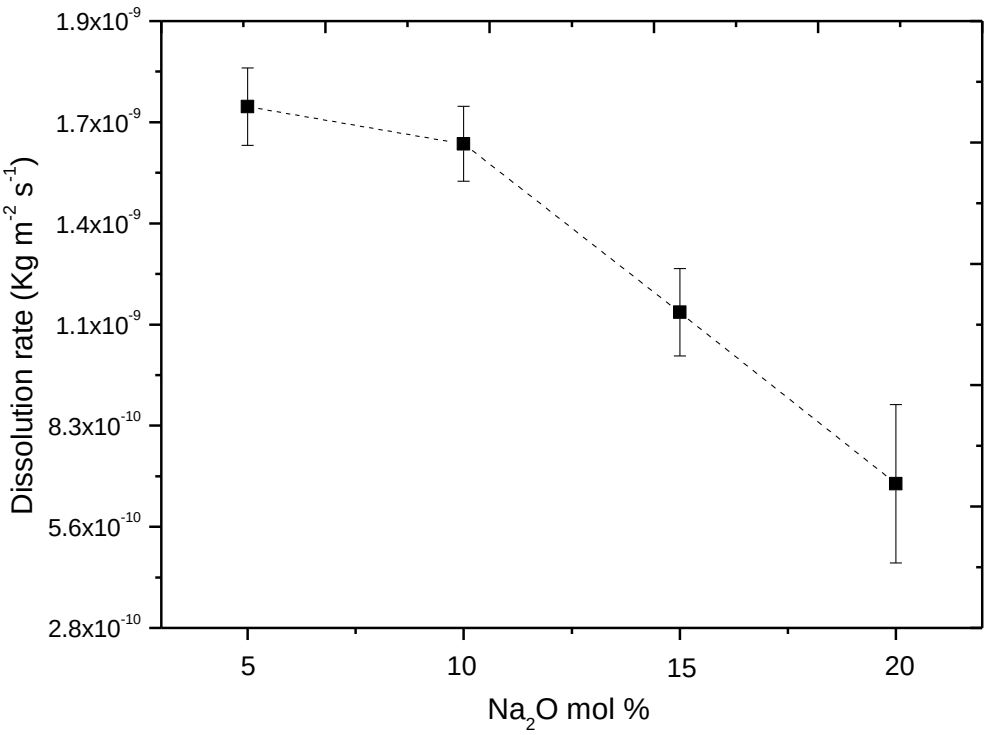
1.9x10-9
1.7x10-9
1.4x10-9
1.1x10-9
8.3x10-10
5.6x10-10
2.8x10-10
Dissolution rate (Kg m-2 s-1)
5
10
15
20
Na2O mol %

Figure 7

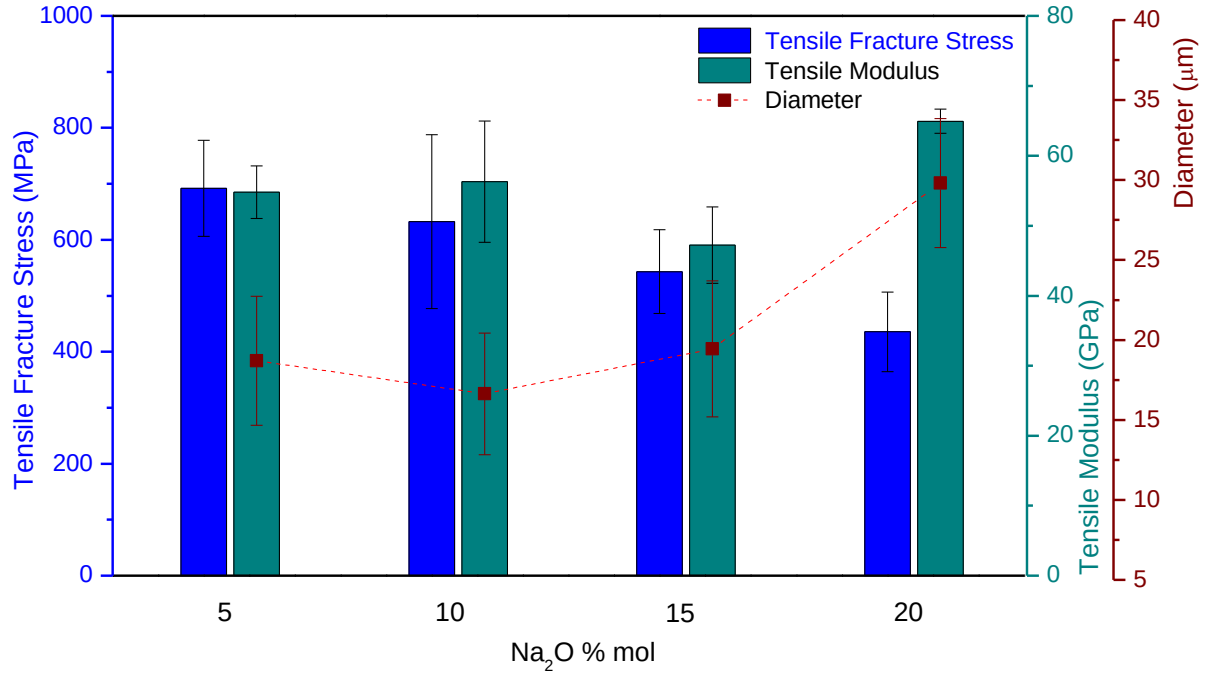
Tensile Fracture Stress
Tensile Modulus
Diameter
Tensile Fracture Stress (MPa)
Tensile Modulus (GPa)
Diameter (μm)
Na2O % mol
0
200
400
600
800
1000
0
20
40
60
80
5
10
15
20
5
10
15
20
25
30
35
40

Figure 8

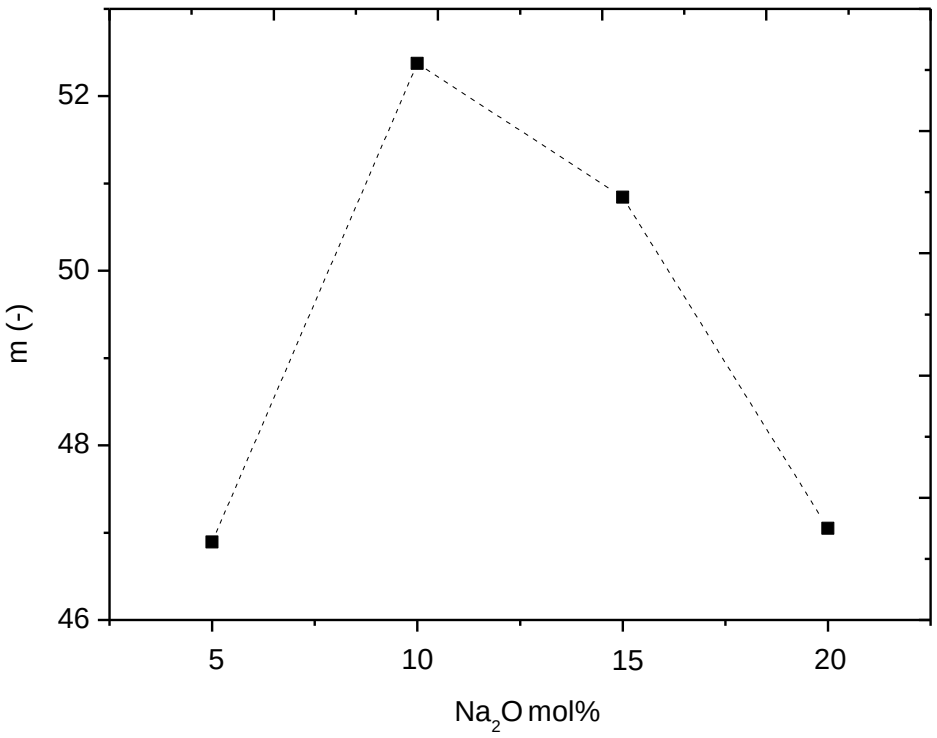

Figure 9

Table 1

Glass code	δ_{CS} ^{23}Na (ppm)	C_Q (MHz)
x=5	-12.20	2.32
x=10	-11.83	2.27
x=15	-10.81	2.29
x=20	-8.53	2.32

Table 2

Glass composition	Glass code	δ_{CSA} ^{31}P Q^2 (ppm) bulk glass	δ_{CSA} ^{31}P Q^2 (ppm) glass fibres
$5Na_2O.16CaO.24MgO.55P_2O_5$	x=5	-139	-136
$10Na_2O.16CaO.24MgO.50P_2O_5$	x=10	-131	-130
$15Na_2O.16CaO.24MgO.45P_2O_5$	x=15	-131	-130
$20Na_2O.16CaO.24MgO.40P_2O_5$	x=20	-123	-123

Table 3

Glass code	Tensile Fracture Stress (MPa)	σ_0(MPa)	m (Weibull modulus)
x=5	692±86	737	9.33
x=10	632±155	699	5.42
x=15	543±75	574	9.51
x=20	436±71	472	6.65